

Upper critical field and thermally activated flux flow in single crystalline $\text{Tl}_{0.58}\text{Rb}_{0.42}\text{Fe}_{1.72}\text{Se}_2$

L. Jiao,¹ Y. Kohama,² J. L. Zhang,¹ H. D. Wang,^{1,3} B. Maiorov,² F. F. Balakirev,² Y. Chen,¹ L. N. Wang,¹ T. Shang,¹ M. H. Fang,¹ and H. Q. Yuan^{1,*}

¹*Department of Physics, Zhejiang University, Hangzhou, Zhejiang 310027, China*

²*Los Alamos National Laboratory, Los Alamos, NM 87545, USA*

³*Department of Physics, Hangzhou Normal University, Hangzhou, Zhejiang 310036, China*

(Dated: March 24, 2019)

The upper critical field $\mu_0 H_{c2}(T_c)$ of $\text{Tl}_{0.58}\text{Rb}_{0.42}\text{Fe}_{1.72}\text{Se}_2$ single crystals has been determined by means of measuring the electrical resistivity in both a pulsed magnetic field ($\sim 60\text{T}$) and a DC magnetic field ($\sim 14\text{T}$). It is found that H_{c2} linearly increases with decreasing temperature for $\mathbf{H} \parallel c$, reaching $\mu_0 H_{c2}^{\mathbf{H} \parallel c}(0\text{K}) \simeq 60\text{T}$. On the other hand, a larger $\mu_0 H_{c2}(0\text{K})$ with a strong convex curvature is observed for $\mathbf{H} \perp c$ ($\mu_0 H_{c2}^{\mathbf{H} \perp c}(18\text{K}) \simeq 60\text{T}$). This compound shows a moderate anisotropy of the upper critical field around T_c , but decreases with decreasing temperature. Analysis of the upper critical field based on the Werthamer-Helfand-Hohenberg (WHH) method indicates that $\mu_0 H_{c2}(0\text{K})$ is orbitally limited for $\mathbf{H} \parallel c$, but the effect of spin paramagnetism may play an important role on the pair breaking for $\mathbf{H} \perp c$. All these experimental observations remarkably resemble those of the iron pnictide superconductors, suggesting a unified scenario for the iron-based superconductors. Moreover, the superconducting transition is significantly broadened upon applying a magnetic field, indicating strong thermal fluctuation effects in the superconducting state of $\text{Tl}_{0.58}\text{Rb}_{0.42}\text{Fe}_{1.72}\text{Se}_2$. The derived thermal activation energy for vortex motion is compatible with those of the 1111-type iron pnictides.

PACS numbers: 74.25.Op; 71.35.Ji; 74.70.Xa

I. INTRODUCTION

The newly discovered Fe-based superconductors (FeSCs) share many similarities to the high T_c cuprates,¹ e.g., both showing a relatively high superconducting transition temperature T_c and possessing a layered crystal structure. It is, therefore, natural to compare these two classes of superconductors, which might help unveil the puzzles of high T_c superconductivity. However, significantly distinct properties have been demonstrated in the FeSCs,¹ including that (i) most of the parent compounds of FeSCs are typical ‘bad metal’ instead of a Mott insulator as found in the cuprates; (ii) the FeSCs are a multi-band system, which seem to favor a s^\pm pairing state rather than a d -wave state; (iii) both the FeSCs and the cuprates possess a very large upper critical field, but the FeSCs show nearly isotropic H_{c2} at low temperatures in despite of their layered crystal structures. Clarification of the electronic coupling strength in FeSCs is the basis for establishing a pertinent theory of superconductivity. Various approaches, either based on the Fermi surface nesting² or started from the proximity to a Mott insulator³ were initially proposed to reveal the physics of iron pnictides, but no consensus has been reached. Recently, dual characters of localized and itinerant 3d-electrons were theoretically proposed⁴ and experimentally shown in some iron pnictides.^{5,6} To reveal the nature of magnetism and superconductivity in FeSCs and compare it with the high T_c cuprates, it remains highly desired to search for FeSCs nearby a Mott insulator.

Very recently a new class of FeSCs, AFe_xSe_2 ($\text{A}=\text{K}$,⁷ Cs ,⁸ Rb ,⁹ $(\text{Tl}_{1-y}\text{K}_y)$ ¹⁰ and $(\text{Tl}_{1-y}\text{Rb}_y)$ ¹¹), were discov-

ered with T_c up to $\sim 33\text{K}$. Remarkably different from the iron pnictides, superconductivity in iron selenides seems to develop from an antiferromagnetic Mott insulator with a rather high Néel temperature.^{10–15} In these compounds, one may tune the interplay of superconductivity and magnetism by changing the Fe-vacancy order.^{10,14,15} Furthermore, the reported ARPES experiments on iron selenides showed that an isotropic superconducting gap emerges around the electron pocket at M point but the hole band centered at Γ point sinks below the Fermi level.^{16–18} This is in sharp contrast to that of the iron pnictide superconductors, in which both hole- and electron-pockets, connected with a nesting wave vector, were experimentally observed.¹⁹ It is, therefore, of great interest to find out whether the iron selenide superconductors represent a new type of FeSCs (e.g., similar to the high T_c cuprates) or remain similar to other iron pnictides. In any case, the iron selenide superconductors may provide an alternative example for studying the pairing mechanisms of high T_c superconductivity, in particular for the FeSCs. To elucidate the above issues, it is highly important to compare the main superconducting parameters of the iron selenides with those of the iron pnictides, and also among the iron selenide series.

In this article, we report measurements of the electrical resistivity in both a pulsed magnetic field and a DC magnetic field for the single-crystalline $\text{Tl}_{0.58}\text{Rb}_{0.42}\text{Fe}_{1.72}\text{Se}_2$. It is found that $\text{Tl}_{0.58}\text{Rb}_{0.42}\text{Fe}_{1.72}\text{Se}_2$ shows a very large upper critical field ($\mu_0 H_{c2}^{\mathbf{H} \parallel c}(0\text{K}) \simeq 60\text{T}$, $\mu_0 H_{c2}^{\mathbf{H} \perp c}(18\text{K}) \simeq 60\text{T}$) with a moderate anisotropic parameter γ ($\gamma = H_{c2}^{\mathbf{H} \perp c}/H_{c2}^{\mathbf{H} \parallel c}$), remarkably resembling those of iron pnictide superconductors.^{20–25} On the other hand, the super-

conducting transition of $\text{Tl}_{0.58}\text{Rb}_{0.42}\text{Fe}_{1.72}\text{Se}_2$ is substantially broadened in a magnetic field, indicating significant contributions of thermally activated flux flow in the vortex state.

II. EXPERIMENTAL METHODS

Single crystals of $\text{Tl}_{0.58}\text{Rb}_{0.42}\text{Fe}_{1.72}\text{Se}_2$ were synthesized by using a Bridgeman method.¹¹ The X-ray diffraction (XRD) identified the derived samples as a single phase with a tetragonal ThCr_2Si_2 crystal structure. The actual composition of the crystals was determined by energy dispersive X-ray spectrometer (EDXS). Magnetic field dependence of the electrical resistivity, $\rho(H)$, was measured up to 60T using a typical 4-probe method in a capacitor-bank-driven pulsed magnet. The experimental data were recorded on a digitizer using a custom designed high-resolution, low-noise synchronous lock-in technique. In order to minimize the eddy-current heating caused by the pulsed magnetic field, very small crystals were cleaved off along the ab -plane from the as-grown samples. The electrical resistivity in a DC magnetic field (0–14T) was measured in an Oxford Instruments HELIOX VL system using a Lakeshore AC Resistance Bridge and the angular dependence of the electrical resistivity was performed in a Quantum Design (QD) Physical Properties Measurement System (9T PPMS). Angular linear (ρ) transport measurements were carried out using the maximum Lorentz force configuration ($\mathbf{J} \perp \mathbf{H}$), with \mathbf{H} applied at an angle θ from the c axis of the crystal (see the inset of Fig. 5).

III. THE UPPER CRITICAL FIELD AND ITS ANISOTROPY

In Fig. 1, we show the temperature dependence of the electrical resistivity at zero field for $\text{Tl}_{0.58}\text{Rb}_{0.42}\text{Fe}_{1.72}\text{Se}_2$ (#1). One can see that the resistivity $\rho(T)$ shows a hump around 154K, changing from semiconducting to metallic behavior upon cooling down from room temperature. Such a hump in $\rho(T)$ has been widely observed in the iron selenides^{7–12,26} and its position can be tuned either by doping¹² or pressure.²⁶ The origin of the hump and its relation with superconductivity remain unclear. A very sharp superconducting transition shows up around $T_c=33\text{K}$, indicating a high quality of the sample. Note that we have totally measured four samples cut from the same batch in this context and their T_c only vary slightly from 32.9K to 33.3K, indicating a good reproducibility of the superconducting properties in these samples.

Fig. 2 and Fig. 3 show the temperature- and the magnetic-field-dependence of the electrical resistivity for $\text{Tl}_{0.58}\text{Rb}_{0.42}\text{Fe}_{1.72}\text{Se}_2$, respectively. In order to study the anisotropic behavior, the electrical resistivity was measured with field perpendicular (a) and parallel (b) to the c -axis. The magnetic field is applied up to 14T for

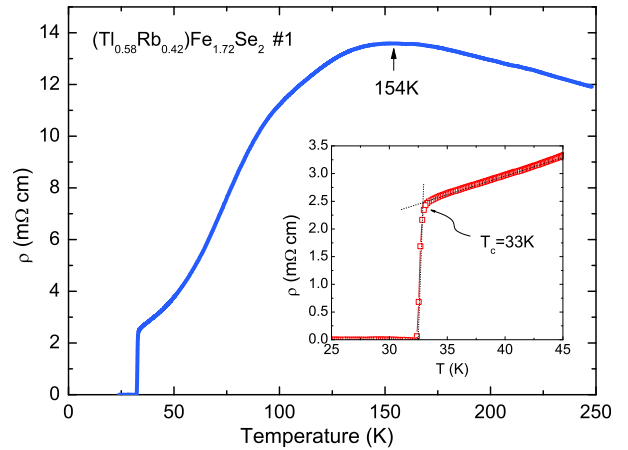


FIG. 1: (Color online) Temperature dependence of the electrical resistivity $\rho(T)$ at $H = 0$ for $\text{Tl}_{0.58}\text{Rb}_{0.42}\text{Fe}_{1.72}\text{Se}_2$ (#1). The inset enlarges the section at the superconducting transition, where $T_c \simeq 33\text{K}$ is determined from the intersection point of the two dotted lines as shown in the figure.

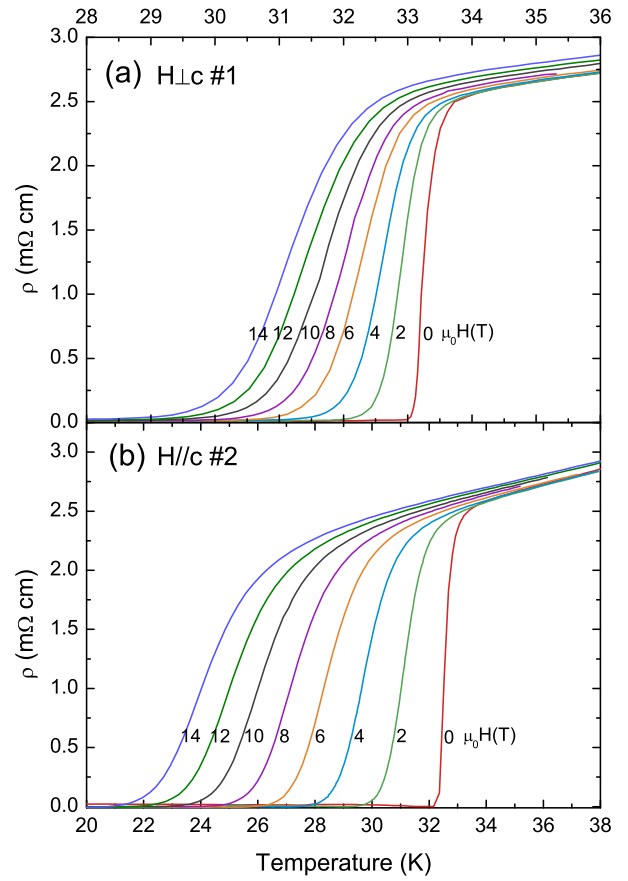


FIG. 2: (Color online) Temperature dependence of the electrical resistivity $\rho(T)$ for $\text{Tl}_{0.58}\text{Rb}_{0.42}\text{Fe}_{1.72}\text{Se}_2$ (#1 and #2) measured in DC fields up to 14T: (a) $\mathbf{H} \perp c$; (b) $\mathbf{H} \parallel c$.

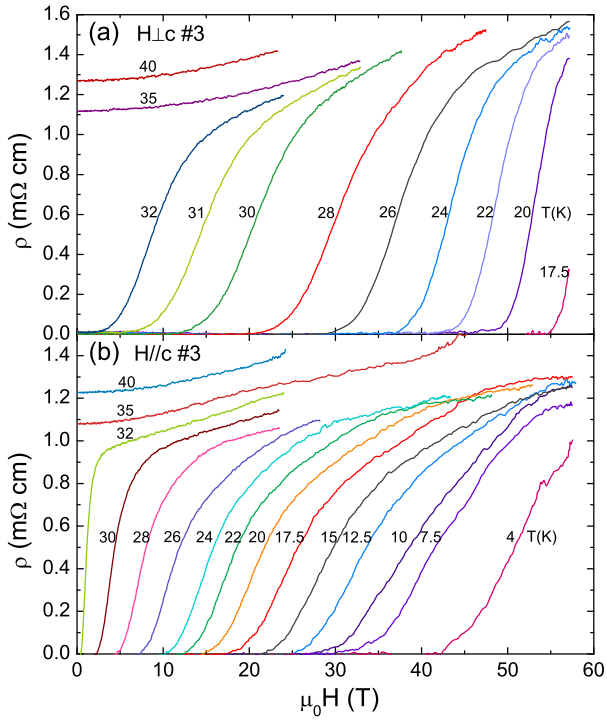


FIG. 3: (Color online) Magnetic field dependence of the electrical resistivity $\rho(H)$ at various temperatures for $\text{Tl}_{0.58}\text{Rb}_{0.42}\text{Fe}_{1.72}\text{Se}_2$ (#3): (a) $\mathbf{H} \perp c$; (b) $\mathbf{H} \parallel c$.

the DC field (Fig. 2) and to 60T for the pulsed magnetic field (Fig. 3). Obviously, the superconducting transition eventually shifts to lower temperature upon applying a magnetic field. However, superconductivity is remarkably robust against the magnetic field in $\text{Tl}_{0.58}\text{Rb}_{0.42}\text{Fe}_{1.72}\text{Se}_2$; T_c remains finite even at a field of 60T, in particular for the case of $\mathbf{H} \perp c$. Besides the robustness of superconductivity to the magnetic field, one can see that the superconducting transition is significantly broadened upon applying a magnetic field, showing a tail structure at low temperature. For example, the width of the superconducting transition, defined from the temperatures at which the resistivity reaches 90% and 10% of the value at T_c , is as small as 0.3K at zero field, but increases to 2K and 3.6K for $\mathbf{H} \perp c$ and $\mathbf{H} \parallel c$ at 14T, respectively. Similar features were also observed in some 1111-type iron pnictides.^{27–29} We will argue later that such behavior might be attributed to the thermally activated flux flow in the vortex state. In the normal state, $\text{Tl}_{0.58}\text{Rb}_{0.42}\text{Fe}_{1.72}\text{Se}_2$ shows significant positive magnetoresistance for both $\mathbf{H} \parallel c$ and $\mathbf{H} \perp c$. It is noted that, in iron pnictides, the magnetoresistance becomes very large while entering the magnetic state, but is negligible in the non-magnetic state.⁵ One possibility for the occurrence of such a large magnetoresistance in $\text{Tl}_{0.58}\text{Rb}_{0.42}\text{Fe}_{1.72}\text{Se}_2$ might be related to its magnetic ordering at high temperature.^{14,15}

The upper critical field $\mu_0 H_{c2}(T_c)$ of $\text{Tl}_{0.58}\text{Rb}_{0.42}\text{Fe}_{1.72}\text{Se}_2$ is shown in Fig. 4, in which

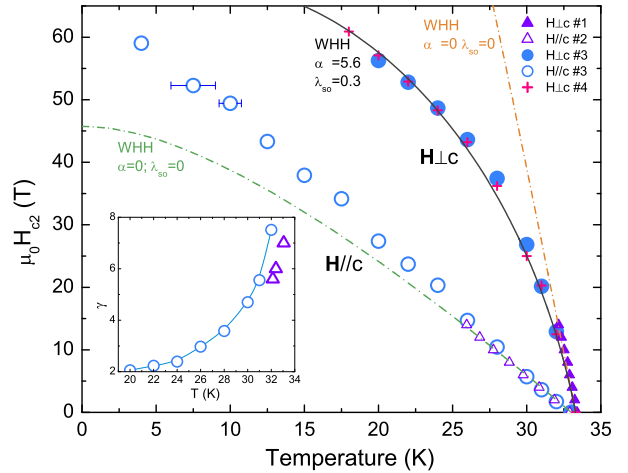


FIG. 4: (Color online) The upper critical field $\mu_0 H_{c2}(T_c)$ for $\text{Tl}_{0.58}\text{Rb}_{0.42}\text{Fe}_{1.72}\text{Se}_2$. Symbols of the open circle (\circ), filled circle (\bullet) and cross (\times) represent the data obtained in a pulsed magnetic field and the triangles (\triangle and \blacktriangle) denote those measured in a DC magnetic field. Note that samples #3 and #4 were measured in a pulsed field, but only sample #3 was successfully measured for both $\mathbf{H} \perp c$ and $\mathbf{H} \parallel c$. The inset shows the temperature dependence of the anisotropic parameter $\gamma(T)$.

various symbols represent either different samples or different field orientations as marked in the plot. Considering the broadening of the superconducting transition in a magnetic field, we determine the critical fields $\mu_0 H_{c2}$ (in the case of pulsed field) or the critical temperatures T_c (in the case of DC field) from the superconducting onsets as described in the inset of Fig. 1, i.e., the intersection points of the resistive curves in the normal state and the superconducting states. One can see that all the investigated samples demonstrate quantitatively same behavior of $\mu_0 H_{c2}(T_c)$, independent of the detailed experimental methods. The upper critical field $\mu_0 H_{c2}^{\mathbf{H} \parallel c}(T_c)$ linearly increases with decreasing temperature, reaching a value of $\mu_0 H_{c2}^{\mathbf{H} \parallel c}(0\text{K}) \simeq 60\text{T}$. On the other hand, $\mu_0 H_{c2}^{\mathbf{H} \perp c}(T_c)$ shows a convex shape with a much larger value of $\mu_0 H_{c2}$ at low temperature. It is noted that our results are consistent with those of $\text{K}_{0.8}\text{Fe}_{1.76}\text{Se}_2$ ³⁰ and $\text{K}_{0.76}\text{Fe}_{1.61}\text{Se}_{0.96}\text{S}_{1.04}$;³¹ the former was measured using a tunnel-diode resonator technique in a pulsed magnetic field and the latter was only measured up to a field of 9T.

In a superconductor, the Cooper pairs can be destroyed by the following two mechanisms in a magnetic field: (i) the orbital pair breaking due to the Lorentz force acting via the charge on the momenta of the paired electrons (orbital limit); (ii) the Zeeman effect aligning the spins of the two electrons with the applied field (Pauli paramagnetic limit). According to the WHH method, the orbital-limiting upper critical field $\mu_0 H_{c2}^{orb}(0\text{K})$ for a single band BCS superconductor is determined by the initial

slope of $\mu_0 H_{c2}(T_c)$ at T_c , i.e.³²

$$\mu_0 H_{c2}^{orb}(0K) = -0.69 T_c (dH_{c2}/dT) |_{T=T_c}, \quad (1)$$

which value may depend on the field orientations. The Pauli paramagnetic limiting field for weakly coupled BCS superconductors is given by³³

$$\mu_0 H_{c2}^p(0K)[T] = 1.86 T_c[K]. \quad (2)$$

While the upper critical field is usually restricted by the orbital limit in conventional superconductors, the spin paramagnetic effect may play an important role in pair breaking in some unconventional superconductors. $Tl_{0.58}Rb_{0.42}Fe_{1.72}Se_2$ reveals a relatively large and anisotropic initial slope of $\mu_0 H_{c2}(T_c)$ near T_c , which reaches a value of $-12T/K$ and $-2T/K$ for $\mathbf{H} \perp c$ and $\mathbf{H} \parallel c$, respectively. Following Eq. 1, one can derive the orbitally limited upper critical field, which gives $\mu_0 H_{c2}^{orb}(0K) = 273T$ for $\mathbf{H} \perp c$ and $45T$ for $\mathbf{H} \parallel c$. As shown in Fig. 4, $\mu_0 H_{c2}^{orb}(0K)$ considerably exceeds the experimental value of $\mu_0 H_{c2}(0K)$ for $\mathbf{H} \perp c$, but lightly falls below the corresponding $\mu_0 H_{c2}(0K)$ for $\mathbf{H} \parallel c$. On the other hand, Eq. 2 gives a Pauli paramagnetic limiting field of $\mu_0 H_{c2}^p(0K) \approx 60T$ in terms of the BCS theory. Thus, it is likely that the upper critical field is limited by orbital effect for $\mathbf{H} \parallel c$, but by spin paramagnetic effect for $\mathbf{H} \perp c$. In order to further look into this point, we fitted the experimental data of $\mu_0 H_{c2}(T_c)$ by the WHH model,³² in which the effects of both orbital- and spin-pair breaking are considered (see Fig. 4). In this model, α and λ_{so} are the fitting parameters; α is the Maki parameter, which represents the relative strength of orbital and spin pair-breaking, and λ_{so} is the spin-orbit scattering constant. As shown in Fig. 4, the upper critical field $\mu_0 H_{c2}(T_c)$ for both $\mathbf{H} \parallel c$ and $\mathbf{H} \perp c$ are not well described by the WHH method while ignoring the spin effect (see the dot dashed lines with $\alpha=0$ and $\lambda_{so}=0$). The enhancement of $\mu_0 H_{c2}^{\mathbf{H} \parallel c}(T_c)$ at low temperature is likely attributed to its multi-band electronic structure as discussed in other FeSCs.²⁵ $\mu_0 H_{c2}^{\mathbf{H} \perp c}(T_c)$ can be well fitted by the WHH model after considering the spin effect (see the solid line in Fig. 4), which gives $\alpha=5.6$ and $\lambda_{so}=0.3$. Such a large value of α indicates that the spin paramagnetism may play an important role on suppressing superconductivity for $\mathbf{H} \perp c$. In the case of a cylinder-like Fermi surface, the open electron orbits along the c -axis make the orbital limiting upper critical field unlikely. This indeed agrees with the enhanced anisotropic parameter γ in $Tl_{0.58}Rb_{0.42}Fe_{1.72}Se_2$ (see below), which suggests a more two-dimensional band structure in this compound. Nevertheless, these properties are quite similar to those observed in iron pnictide superconductors,²⁰⁻²⁵ in particular to that of $LiFeAs$ ²³, indicating uniform behavior of the upper critical field in the FeSCs.

Temperature dependence of the anisotropic parameter $\gamma(T)$ is shown in the inset of Fig. 4 for $Tl_{0.58}Rb_{0.42}Fe_{1.72}Se_2$. The anisotropic parameter reaches $\gamma \sim 8$ near T_c and decreases monotonically to 2

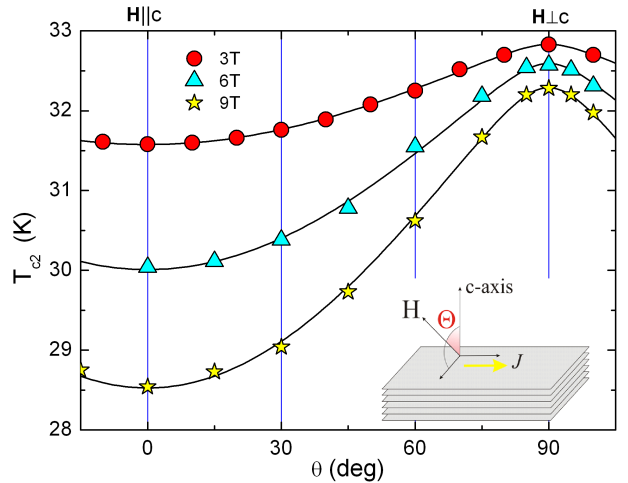


FIG. 5: (Color online) The angular dependence of the superconducting critical temperature $T_c(\theta)$ at magnetic fields of $\mu_0 H=3T$, $6T$ and $9T$. The solid lines show the fittings to Eq. 4.

at 20K, showing that $Tl_{0.58}Rb_{0.42}Fe_{1.72}Se_2$ has a relatively large anisotropy of the upper critical field among the FeSCs. Note that samples #1 and #2 measured in a DC field exhibit similar anisotropic behavior but with a slightly smaller γ . Such a deviation might result from the weak sample dependence of γ and/or the slight deviation of the field orientation in different measurements. In order to further characterize the nature of the anisotropy in $Tl_{0.58}Rb_{0.42}Fe_{1.72}Se_2$, we measured the angular dependence of the electrical resistivity $\rho(T)$ at various magnetic fields. Fig. 5 plots the angular dependence of $T_c(\theta)$, where θ is the angle between the magnetic field and the c -axis of the sample.

According to the single band anisotropic Ginzburg-Landau (G-L) theory,^{34,35} the angular dependence of the upper critical field can be scaled by:

$$\mu_0 H_{c2}^{CL}(\theta) = \mu_0 H_{c2} / \sqrt{\cos^2(\theta) + \gamma^{-2} \sin^2(\theta)}, \quad (3)$$

where $\gamma = (m_{ab}/m_c)^{1/2} = H_{c2}^{\mathbf{H} \perp c} / H_{c2}^{\mathbf{H} \parallel c}$. Here m_{ab} and m_c are the effective masses of electrons for the in-plane and out-of-plane motion, respectively. In the case that H_{c2} is a linear function of temperature, the angular dependence of $\mu_0 H_{c2}(\theta)$ can be converted to that of T_{c2} by:³⁶

$$T_{c2}(\theta) = T_{c0} + H / (\partial H_{c2}^{\mathbf{H} \parallel c} / \partial T) \sqrt{\cos^2(\theta) + \gamma^{-2} \sin^2(\theta)}, \quad (4)$$

where T_{c0} is the zero field superconducting transition temperature and H is the applied magnetic field. In our case, the upper critical field near T_c indeed shows nearly linear temperature dependence for both $\mathbf{H} \perp c$ and $\mathbf{H} \parallel c$. Therefore, one can estimate the anisotropic parameter γ from the angular dependence of $T_{c2}(\theta)$. The use of a single band anisotropic model to describe the angular dependence of H_{c2} in a multiband system is appropriate at high T and low H , since the predictions of the two-band model

and a single band are almost identical near T_c as calculated in Ref. 37 and observed in Ref. 21. Indeed, $T_c(\theta)$ can be nicely fitted by Eq. 4 (see the solid lines in Fig.5), indicating that, at least in the low field region, $T_c(\theta)$ can be described by the G-L theory and the anisotropic upper critical field is attributed to the effective mass anisotropy in strongly coupled layered superconductors. We obtained the following parameters from above fitting: $\gamma=8.5, 7.3$ and 6.3 for $\mu_0 H=3\text{T}, 6\text{T}$ and 9T , respectively. The parameters of $\gamma(H)$ are quantitatively consistent with those obtained from the pulsed field measurements after considering the relation of $\mu_0 H_{c2}(T_c)$. Previously reported values for the anisotropic parameter γ in FeSCs are smaller than 6 near T_c .²⁰⁻²⁵ Our finding of $\gamma\sim 8$ near T_c in $\text{Tl}_{0.58}\text{Rb}_{0.42}\text{Fe}_{1.72}\text{Se}_2$ suggests that this compound might have a more two-dimensional character.

In comparison, the iron selenides show intrinsically similar properties of the upper critical field to the iron pnictide superconductors,²⁰⁻²⁵ but with a slightly enhanced anisotropy. These findings suggest that all these FeSCs might share the same characters of superconductivity. This is surprising because the electronic structure and the normal state of iron selenides seem to be very unique among the FeSCs. For example, both hole pockets and electron pockets are observed in iron pnictides,¹⁹ but the hole pocket is absent in iron selenides.¹⁶⁻¹⁸ The nesting between the hole pockets and the electron pockets was regarded as a prerequisite factor for the forming of s^\pm paring state,³⁸ a widely accepted proposal for the iron pnictide superconductors. Our findings of the uniform behavior of $\mu_0 H_{c2}(T_c)$ in iron pnictides and selenides, therefore, urge to check whether the missing of hole pockets in iron selenides is intrinsic or masked by other experimental factors. If it is intrinsic, one probably needs to reconsider the order parameters and the pairing mechanism of FeSCs in a unified picture.

IV. THERMALLY ACTIVATED FLUX FLOW

As already mentioned above, the superconducting transition is significantly broadened in $\text{Tl}_{0.58}\text{Rb}_{0.42}\text{Fe}_{1.72}\text{Se}_2$ upon applying a magnetic field (see Fig. 2 and Fig. 3). Similar features were previously observed in other layered superconductors, including the cuprates^{39,40} and 1111-type iron pnictides,²⁷⁻²⁹ which were interpreted in terms of the energy dissipation caused by vortices motion. Indeed, the presence of a vortex liquid phase is the result of a fairly larger anisotropy ($\gamma\sim 8$) that will result in a much higher Ginzburg number, $Gi=(\gamma T_c/H_c^2 \xi_c^3)^2$, than that typically found in a 122-type iron pnictides ($\gamma\simeq 2$) where the range of vortex liquid state is very narrow.⁴¹

According to the thermally activated flux flow model (TAFF),⁴² the resistivity $\rho(T, H)$ can be expressed as:

$$\rho = (2\nu_0 LH/J) \sinh[JHVL/T] e^{-J_{c0}HVLT}, \quad (5)$$

where ν_0 is an attempt frequency for a flux bundle hop-

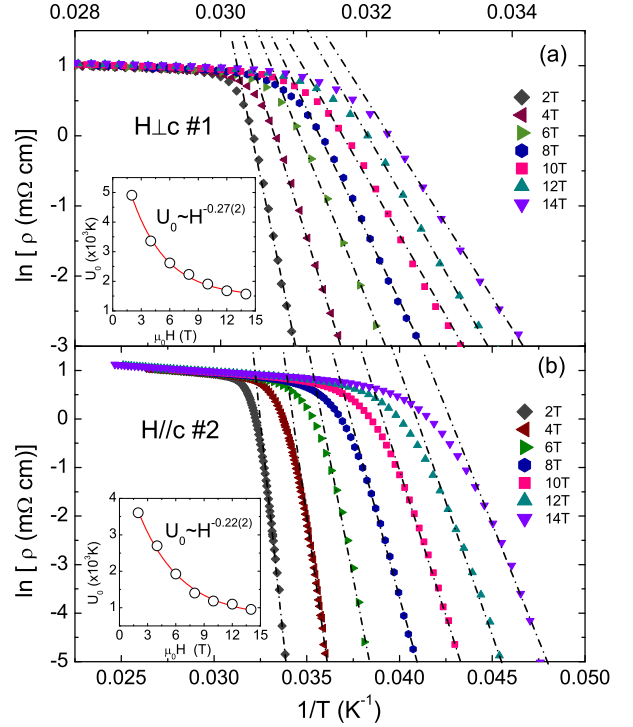


FIG. 6: (Color online) Arrhenius plot of $\text{Tl}_{0.58}\text{Rb}_{0.42}\text{Fe}_{1.72}\text{Se}_2$ at various magnetic fields: (a) $\mathbf{H}\perp c$; (b) $\mathbf{H}\parallel c$. The inset shows the thermally activated energy, $U_0(H)$, obtained from the slope of the Arrhenius plot. The solid lines are fitted to $U_0(H) \approx H^{-n}$ with $n=0.27\pm 0.02$ and 0.22 ± 0.02 for $\mathbf{H}\perp c$ and $\mathbf{H}\parallel c$, respectively.

ping, L is the hopping distance, J is the applied current density, J_{c0} is the critical current density in the absence of flux creep and V is the bundle volume. In the limit of $JHVL/T \ll 1$, Eq. 5 can be expressed as

$$\rho = (2\rho_c U/T) e^{-U/T}, \quad (6)$$

where $U = J_{c0}HVL$ is the thermally activated energy and $\rho_c = \nu_0 LH/J_{c0}$. Assuming that $2\rho_c U/T$ is a temperature independent constant, noted as ρ_{0f} , and $U = U_0(1 - T/T_c)$, then Eq. 6 can be simplified to the Arrhenius relation:

$$\ln \rho(T, H) = \ln \rho_{0f} - U_0(H)/T. \quad (7)$$

Thus, the apparent activation energy, $U_0(H)$, could be extracted from the slopes of the Arrhenius plots, i.e., the plot of $\ln \rho$ v.s. $1/T$.

In order to study the possible vortex motion in $\text{Tl}_{0.58}\text{Rb}_{0.42}\text{Fe}_{1.72}\text{Se}_2$, we plot the electrical resistivity ρ as a function of $1/T$ in a semi-log scale at various magnetic fields (see Fig. 6). It is clear that the Arrhenius relation holds over a wide temperature range for both $\mathbf{H}\perp c$ and $\mathbf{H}\parallel c$. Following $U_0(H) = -d\ln \rho/d(1/T)$, the apparent activation energy, $U_0(H)$, can then be determined from the slope of the linear parts in Fig. 6. For example, this yields $U_0 \approx 4900\text{K}$ for $\mathbf{H}\perp c$ and 3607K for

$\mathbf{H} \parallel c$ at 2T. The derived values of $U_0(H)$ are plotted as a function of field in the insets of Fig. 6: (a) $\mathbf{H} \perp c$ and (b) $\mathbf{H} \parallel c$, which follow a power law of $U_0(H) \sim H^{-n}$. The fittings give $n=0.27 \pm 0.02$ for $\mathbf{H} \perp c$ and 0.22 ± 0.02 for $\mathbf{H} \parallel c$, indicating that the pinning force changes with the field orientation as a result of the layered crystal structure. The derived values of $U_0(H)$ are slightly larger than those of some 1111-type iron pnictides, e.g. NdFeAsO_{0.7}F_{0.3}²⁷ and CeFeAsO_{0.9}F_{0.1}²⁸ but smaller than those of SmFeAsO_{0.85}²⁹ and YBCO⁴⁰, indicating a moderate pinning force among the cuprates and FeSCs.

V. CONCLUSION

The upper critical field $\mu_0 H_{c2}(T_c)$, its anisotropy $\gamma(T)$ and the vortex motion of the newly discovered Tl_{0.58}Rb_{0.42}Fe_{1.72}Se₂ have been studied by measuring the field-, temperature- and angular- dependence of the electrical resistivity. We found that this compound shows a large upper critical field ($\mu_0 H_{c2}^{\mathbf{H} \parallel c}(0\text{K}) \simeq 60\text{T}$, $\mu_0 H_{c2}^{\mathbf{H} \perp c}(18\text{K}) \simeq 60\text{T}$) with a moderate anisotropy near T_c . The anisotropic parameter decreases with decreasing temperature, reaching $\gamma(20\text{K}) \sim 2$. Analysis based on the WHH model indicates that the upper critical field is orbitally limited for $\mathbf{H} \parallel c$, but is likely limited by the spin paramagnetic effect for $\mathbf{H} \perp c$. These properties remarkably resemble those of iron pnictide superconduc-

tors, suggesting that all the Fe-based superconductors may bear the same characters and, therefore, provide restrictions on the theoretical model. Similar to the cuprates and 1111-series of iron pnictides, thermally activated flux flow might be responsible for the tail structure of the resistive transition below T_c and the derived thermal activation energies are compatible with those of the 1111-type iron pnictides.

Acknowledgments

Work at ZJU was supported by the National Science Foundation of China (grant Nos: 10874146, 10934005, 10974175), the National Basic Research Program of China (973 Program) (2009CB929104, 2011CBA00103), the PCSIRT of the Ministry of Education of China, Zhejiang Provincial Natural Science Foundation of China, and the Fundamental Research Funds for the Central Universities. Work at LANL was performed under the auspices of the National Science Foundation, the Department of Energy, and the State of Florida. BM was supported by the U.S. Department of Energy, Basic Energy Sciences, Materials Sciences and Engineering Division.

References

- * Electronic address: hqyuan@zju.edu.cn
- ¹ For reviews, see, e.g., Z. A. Ren, and Z. X. Zhao, *Adv. Mater.* **21**, 4584 (2009); D. C. Johnston, *Adv. Phys.* **59**, 803 (2010); J. Paglione, and R. L. Greene, *Nat. Phys.* **6**, 645 (2010); P. M. Aswathy, J. B. Anooja, P. M. Sarun, and U. Syamaprasad, *Supercond. Sci. Technol.* **23**, 073001 (2010).
- ² J. Dong, H. J. Zhang, G. Xu, Z. Li, G. Li, W. Z. Hu, D. Wu, G. F. Chen, X. Dai, J. L. Luo, Z. Fang, and N. L. Wang, *Europhys. Lett.* **83**, 27006 (2008); D. J. Singh, and M. H. Du, *Phys. Rev. Lett.* **100**, 237003 (2008).
- ³ Q. Si, and E. Abrahams, *Phys. Rev. Lett.* **101**, 076401 (2008); K. Seo, B. A. Bernevig, and J. P. Hu, *Phys. Rev. Lett.* **101**, 506404 (2008); J. H. Dai, Q. M. Si, J. X. Zhu, and E. Abrahams, *Proc. Natl. Acad. Sci.* **106**, 4118 (2009).
- ⁴ S. P. Kou, T. Li, and Z. Y. Weng, *Europhys. Lett.* **88**, 17010 (2009); M. D. Johannes, and I. I. Mazin, *Phys. Rev. B* **79**, 220510(R) (2009); L. de'Medici, S. R. Hassan, M. Capone, and X. Dai, *Phys. Rev. Lett.* **102**, 126401 (2009).
- ⁵ H. Q. Yuan, L. Jiao, F. F. Balakirev, J. Singleton, C. Setty, J. P. Hu, T. Shang, L. J. Li, G. H. Cao, Z. A. Xu, B. Shen, and H. H. Wen, arXiv:cond-mat/1102.5476 (2011).
- ⁶ S. J. Moon, J. H. Shin, D. Parker, W. S. Choi, I. I. Mazin, Y. S. Lee, J. Y. Kim, N. H. Sung, B. K. Cho, S. H. Khim, J. S. Kim, K. H. Kim, and T. W. Noh, *Phys. Rev. B* **81**, 205114 (2010).
- ⁷ J. G. Guo, S. F. Jin, G. Wang, S. C. Wang, K. X. Zhu, T. T. Zhou, M. He, and X. L. Chen, *Phys. Rev. B* **82**, 180520 (2010).
- ⁸ A. Krzton-Maziopa, Z. Shermadini, E. Pomjakushina, V. Pomjakushin, M. Bendele, A. Amato, R. Khasanov, H. Luetkens, and K. Conder, *J. Phys.: Condens. Matter* **23**, 052203 (2011).
- ⁹ A. F. Wang, J. J. Ying, Y. J. Yan, R. H. Liu, X. G. Luo, Z. Y. Li, X. F. Wang, M. Zhang, G. J. Ye, P. Cheng, Z. J. Xiang, and X. H. Chen *Phys. Rev. B* **83**, 060512 (2011).
- ¹⁰ M. H. Fang, H. D. Wang, C. H. Dong, Z. J. Li, C. M. Feng, J. Chen, and H. Q. Yuan, *Europhys. Lett.* **94**, 27009 (2011).
- ¹¹ H. D. Wang, C. H. Dong, Z. J. Li, Q. H. Mao, S. S. Zhu, C. M. Feng, H. Q. Yuan, and M. H. Fang, *Europhys. Lett.* **93**, 47004 (2011).
- ¹² R. H. Liu, X. G. Luo, M. Zhang, A. F. Wang, J. J. Ying, X. F. Wang, Y. J. Yan, Z. J. Xiang, P. Cheng, G. J. Ye, Z. Y. Li, and X. H. Chen, *Europhys. Lett.* **94**, 27008 (2011).
- ¹³ Z. Shermadini, A. Krzton-Maziopa, M. Bendele, R. Khasanov, H. Luetkens, K. Conder, E. Pomjakushina, S. Weyeneth, V. Pomjakushin, O. Bossen, and A. Amato, *Phys. Rev. Lett.* **106**, 117602 (2011).
- ¹⁴ W. Bao, G. N. Li, Q. Huang, G. F. Chen, J. B. He, M. A. Green, Y. Qiu, D. M. Wang, and J. L. Luo, arXiv:cond-mat/1102.3674 (2011); W. Bao, Q. Huang, G. F. Chen, M. A. Green, D. M. Wang, J. B. He, X. Q. Wang, and Y. Qiu, arXiv:cond-mat/1102.0830 (2011).
- ¹⁵ Y. J. Yan, M. Zhang, A. F. Wang, J. J. Ying, Z. Y. Li, W. Qin, X. G. Luo, J. Q. Li, J. P. Hu, and X. H. Chen,

arXiv:cond-mat/1104.4941 (2011).

¹⁶ Y. Zhang, L. X. Yang, M. Xu, Z. R. Ye, F. Chen, C. He, H. C. Xu, J. Jiang, B. P. Xie, J. J. Ying, X. F. Wang, X. H. Chen, J. P. Hu, M. Matsunami, S. Kimura, and D. L. Feng, *Nat. Mat.* **10**, 273 (2011).

¹⁷ X. P. Wang, T. Qian, P. Richard, P. Zhang, J. Dong, H. D. Wang, C.-H. Dong, M. H. Fang, and H. Ding, *Europhys. Lett.* **93**, 57001 (2011).

¹⁸ D. X. Mou, S. Y. Liu, X. W. Jia, J. F. He, Y. Y. Peng, L. Zhao, L. Yu, G. D. Liu, S. L. He, X. L. Dong, J. Zhang, H. D. Wang, C. H. Dong, M. H. Fang, X. Y. Wang, Q. J. Peng, Z. M. Wang, S. J. Zhang, F. Yang, Z. Y. Xu, C. T. Chen, and X. J. Zhou, *Phys. Rev. Lett.* **106**, 107001 (2011).

¹⁹ H. Ding, P. Richard, K. Nakayama, K. Sugawara, T. Arakane, Y. Sekiba, A. Takayama, S. Souma, T. Sato, T. Takahashi, Z. Wang, X. Dai, Z. Fang, G. F. Chen, J. L. Luo, and N. L. Wang, *Europhys. Lett.* **83**, 47001 (2008); V. Brouet, M. Marsi, B. Mansart, A. Nicolaou, A. Taleb-Ibrahimi, P. Le Fèvre, F. Bertran, F. Rullier-Albenque, A. Forget, and D. Colson, *Phys. Rev. B* **80**, 165115 (2009).

²⁰ H. Q. Yuan, J. Singleton, F. F. Balakirev, S. A. Baily, G. F. Chen, J. L. Luo, and N. L. Wang, *Nature* **457**, 565 (2009).

²¹ S. A. Baily, Y. Kohama, H. Hiramatsu, B. Maiorov, F. F. Balakirev, M. Hirano, and H. Hosono, *Phys. Rev. Lett.* **102**, 117004 (2009).

²² M. H. Fang, J. H. Yang, F. F. Balakirev, Y. Kohama, J. Singleton, B. Qian, Z. Q. Mao, H. D. Wang, and H. Q. Yuan, *Phys. Rev. B* **81**, 020509 (2010).

²³ N. Kurita, K. Kitagawa, K. Matsubayashi, A. Kismarardja, E. S. Choi, J. S. Brooks, Y. Uwatoko, S. Uji, and T. Terashima, *J. Phys. Soc. Jpn.* **80**, 013706 (2011); K. Cho, H. Kim, M. A. Tanatar, Y. J. Song, Y. S. Kwon, W. A. Coniglio, C. C. Agosta, A. Gurevich, and R. Prozorov, *Phys. Rev. B* **83**, 060502 (2011); J. L. Zhang, L. Jiao, F. F. Balakirev, X. C. Wang, C. Q. Jin, and H. Q. Yuan, *Phys. Rev. B* **83**, 004500 (2011).

²⁴ H. S. Lee, M. Bartkowiak, J. H. Park, J. Y. Lee, J. Y. Kim, N. H. Sung, B. K. Cho, C. U. Jung, J. S. Kim, and H. J. Lee, *Phys. Rev. B* **80**, 144512 (2009).

²⁵ V. A. Gasparov, L. Drigo, A. Audouard, D. L. Sun, C. T. Lin, S. L. Bud'ko, P. C. Canfield, F. Wolff-Fabris, and J. Wosnitza, arXiv:cond-mat/1104.5619 (2011).

²⁶ J. Guo, X. J. Chen, C. Zhang, J. G. Guo, X. L. Chen, Q. Wu, D. C. Gu, P. W. Gao, X. Dai, L. H. Yang, Ho-kwang Mao, L. L. Sun, and Z. X. Zhao, arXiv:cond-mat/1101.0092 (2011).

²⁷ J. Jaroszynski, F. Hunte, L. Balicas, Y. Jo, I. Raicevic, A. Gurevich, D. C. Larbalestier, F. F. Balakirev, L. Fang, P. Cheng, Y. Jia, and H. H. Wen, *Phys. Rev. B* **78**, 174523 (2008).

²⁸ M. Shahbazi, X. L. Wang, C. Shekhar, O. N. Srivastava, and S. X. Dou, *Supercond. Sci. Technol.* **23**, 10500 (2010).

²⁹ Y. Z. Zhang, Z. A. Ren, and Z. X. Zhao, *Supercond. Sci. Technol.* **22**, 065012 (2009); H. Lee, M. Bartkowiak, J. S. Kim, and H. Lee, *Phys. Rev. B* **82**, 104523 (2010).

³⁰ E. D. Mun, M. M. Altarawneh, C. H. Mielke, V. S. Zapf, R. Hu, S. L. Bud'ko and P. C. Canfield, *Phys. Rev. B* **83**, 100514 (2011).

³¹ H. C. Lei, and C. Petrovic, arXiv:cond-mat/1104.2318 (2011).

³² N. R. Werthamer, E. Helfand, and P. C. Hohenberg, *Phys. Rev.* **147**, 295 (1966).

³³ A. M. Clogston, *Phys. Rev. Lett.* **9**, 266 (1962); B. S. Chandrasekhar, *J. Appl. Phys. Lett.* **1**, 7 (1962).

³⁴ D. R. Tilley, *Proc. Phys. Soc. London* **86**, 289 (1965).

³⁵ G. Blatter, V. B. Geshkenbein, and A. I. Larkin, *Phys. Rev. Lett.* **68**, 875 (1992).

³⁶ U. Welp, W. K. Kwok, G. W. Crabtree, K. G. Vandervoort, and J. Z. Liu, *Phys. Rev. B* **40**, 5263 (1989).

³⁷ A. Gurevich, *Phys. Rev. B* **67**, 184515 (2003).

³⁸ I. I. Mazin, and J. Schmalian, *Phys. C* **469**, 614 (2009).

³⁹ W. K. Kwok, S. Fleshler, U. Welp, V. M. Vinokur, J. Downey, G. W. Crabtree, and M. M. Miller, *Phys. Rev. Lett.* **69**, 3370 (1992).

⁴⁰ T. T. M. Palstra, B. Batlogg, R. B. van Dover, L. F. Schneemeyer, and J. V. Waszczak, *Phys. Rev. B* **41**, 6621 (1990).

⁴¹ B. Maiorov, T. Katase, S. A. Baily, H. Hiramatsu, T. G. Holesinger, H. Hosono and L. Civale *Supercond. Sci. Technol.* **24**, 055007 (2011).

⁴² G. Blatter, M. V. Feigel'Man, V. B. Geshkenbein, A. I. Larkin, and V. M. Vinokur, *Rev. Mod. Phys.* **66**, 1125 (1994).